# NUCLEAR MATTER APPROACH TO THE HEAVY-ION OPTICAL POTENTIAL AND THE PROXIMITY APPROXIMATION

By J. Dąbrowski

Institute for Nuclear Studies, Warsaw*

*(Received September 26, 1989)*

A simple theory of the heavy-ion optical potential $\mathscr{V}$, based on the local density approach and the frozen density model, is used to derive the energy dependent proximity approximation $\mathscr{V}^{\mathrm{P}}$ for the complex potential $\mathscr{V}$. Both $\mathscr{V}$ and $\mathscr{V}^{\mathrm{P}}$ are calculated, and the accuracy of the proximity approximation and of the scaling law implied by the approximation is tested.

PACS numbers: 25.70.—z

## *I. Introduction*

In the present paper, the simple nuclear matter (NM) approach to the heavy-ion (HI) optical potential $\mathscr{V} = \mathscr{V}_{\mathrm{R}} + i\mathscr{V}_{\mathrm{I}}$ presented in [1–3] is compared with the proximity force approximation of Błocki, Randrup, Świątecki, and Tsang [4]. These authors formulate the proximity approximation for vanishing energy of the colliding ions, where $\mathscr{V} = \mathscr{V}_{\mathrm{R}}$. We extend the approximation to non-vanishing energies and to the complex potential $\mathscr{V}$.

The NM approach of [1–3] is based on the local density approximation: the two colliding nuclei are described locally as two interpenetrating nuclear matters moving against each other. For the local density and momentum distribution, the frozen density model is applied. The optical potential $\mathscr{V}$ is defined as the difference between the energies of the overlapping and spatially separated nuclei. The energies are calculated in the energy-density formalism. In a simplified form, the approach was employed a long time ago by Brueckner, Buchler, and Kelly [5]. (Since the pioneering work of Brueckner et al., the approach was applied in several papers quoted in [1–3].) Whereas Brueckner et al. used locally the equilibrium momentum distribution, the momentum distribution applied in [1–3] corresponds to a relative motion of two nuclear matters. This leads to a complex effective two-body interaction, and consequently to a complex optical potential $\mathscr{V}$, whereas the potential calculated by Brueckner et al. was pure real.

In the proximity approximation of [4], the calculation of $\mathscr{V}$, based on the frozen den-

* Address: Instytut Problemów Jądrowych, Hoża 69, 00-681 Warszawa, Poland.

sity approximation, is divided into two steps. In the first step, one calculates the proximity force function $\phi(s)$, i.e., the ineraction potential per unit surface between two semi-infinite slabs of NM as a function of the distance $s$ between the two slabs. In the second step, one approximates $\mathscr{V}$ by a superposition of interaction potentials between two slabs of NM at properly chosen distances $s$. The resulting potential in this approximation is denoted by $\mathscr{V}^{\mathrm{P}}$.

In the present paper, we derive the proximity approximation from the NM approach of [1–3] by introducing in this approach approximations valid for sufficiently large separation of the two ions. We compare the results for $\mathscr{V}^{\mathrm{P}}$ with those obtained for $\mathscr{V}$ (with the same NM approach but without the proximity approximation), and thus test the accuracy of the proximity approximation.

The proximity force function $\phi$ was calculated in [4] for vanishing relative velocity of the two slabs of NM. Consequently, $\phi$ was real, and the resulting $\mathscr{V}^{\mathrm{P}}$ (at zero energy $E$ of the colliding nuclei) was also real. In our NM approach, we take into account the relative velocity of the two slabs and obtain a more general proximity function $\phi$ and proximity potential $\mathscr{V}^{\mathrm{P}}$, which depend on the energy $E$ and are complex for $E > 0$. (The energy dependence of pure real $\phi$ and $\mathscr{V}^{\mathrm{P}}$ was first discussed by Moszkowski [6].)

The paper is organized as follows. In Section 2, the NM approach to the HI optical potential $\mathscr{V}$ is outlined with a more detailed description of the frozen density model which is improved compared to the model applied in [1–3]. In Section 3, we derive from the NM approach the proximity approximation for $\mathscr{V}$, $\mathscr{V}^{\mathrm{P}}$. In Section 4, results obtained for $\mathscr{V}$ and $\mathscr{V}^{\mathrm{P}}$ are presented and the accuracy of the proximity approximation and of the scaling law implied by this approximation is discussed.

## *2. The NM approach to the HI optical potential*

### 2.1. The definition of $\mathscr{V}$

We consider two nuclei, 1 (target) and 2 (projectile) (with masses $M_1$, $M_2$, and with the reduced mass $\mu = M_1M_2/(M_1+M_2)$), moving with the relative momentum $\boldsymbol{K}_{\mathrm{REL}}$ (in units of $\hbar$). We denote by $\boldsymbol{R}$ the relative position vector between the centers of mass of 1 and 2 (directed from 1 to 2). The definition of the optical potential $\mathscr{V}$ as the difference between the energies of the overlapping and spatially separated nuclei 1 and 2 does not depend on the reference frame. As the most convenient one, we choose the rest frame of 1, which we call the "laboratory" (lab) frame (at $R = \infty$, it coincides with the laboratory (LAB) frame of nuceli 1 and 2 with nucleus 1 being the target). In this frame

$$\mathscr{V}(E, R) = \mathscr{E}_{\mathrm{lab}}(K_{\mathrm{REL}}, R) - \hbar^2 K_2^2/2M_2 - \mathscr{E}_{\mathrm{in}}(1) - \mathscr{E}_{\mathrm{in}}(2), \tag{2.1}$$

where $\mathscr{E}_{\mathrm{in}}$ $(i)$ is the intrinsic nuclear energy of the isolated nucleus $i$, $\mathscr{E}_{\mathrm{lab}}$ is the nuclear energy of the total system in the lab frame, and

$$\boldsymbol{K}_2 = (M_2/\mu)\boldsymbol{K}_{\mathrm{REL}} \tag{2.2}$$

is the projectile momentum in the lab frame.

The conservation of the total energy implies that the instantaneous relative momentum $\boldsymbol{K}_{\mathrm{REL}} = \boldsymbol{K}_{\mathrm{REL}}(R)$ (and consequently also the projectile momentum $\boldsymbol{K}_2 = \boldsymbol{K}_2(R)$) is changing with $R$:

$$\hbar^2 K_{\mathrm{REL}}(R)^2/2\mu + \mathscr{V}_{\mathrm{R}}(E, R) + \mathscr{V}_{\mathrm{C}}(R) = \hbar^2 K_{\mathrm{REL}}(\infty)^2/2m = E, \tag{2.3}$$

where $\mathscr{V}_{\mathrm{C}}(R)$ is the Coulomb potential between nuclei 1 and 2, and $E$ is the CMS kinetic energy.

We apply the energy-density formalism, and write $\mathscr{E}_{\mathrm{lab}}$ in the form:

$$\mathscr{E}_{\mathrm{lab}}(K_{\mathrm{REL}}, R) = \int d\boldsymbol{r} H_{\mathrm{lab}}(K_{\mathrm{REL}}, R; \boldsymbol{r}), \tag{2.4}$$

where $H_{\mathrm{lab}}$ is the energy density (in the lab frame) at $\boldsymbol{r}$. For a given distance $R$ between the two nuclei, the system is approximated locally (at each point $\boldsymbol{r}$) by a piece of NM of total density $\varrho$ and with momentum distribution $n(\boldsymbol{k}'_{\mathrm{N}})$. Obviously, we have

$$\varrho = [4/(2\pi)^2] \int d\boldsymbol{k}'_{\mathrm{N}} n(\boldsymbol{k}'_{\mathrm{N}}). \tag{2.5}$$

(We assume that both nuclei 1 and 2 are spin and isospin saturated. Nucleon momenta in the lab frame are denoted by $\boldsymbol{k}'_{\mathrm{N}}$.)

## 2.2. The frozen density model

For $\varrho$ and $n(\boldsymbol{k}'_{\mathrm{N}})$, we apply the frozen density model in which all degrees of freedom are frozen, except for $R$. The total local density of the combined system at $\boldsymbol{r}$ is equal to the sum of the original densities of nuclei 1 and 2:

$$\varrho(\boldsymbol{r}) = \varrho_1(r) + \varrho_2(|\boldsymbol{r} - \boldsymbol{R}|). \tag{2.6}$$

(The origin of the position vector $\boldsymbol{r}$ is the same as that of $\boldsymbol{R}$, i.e., the center of 1. We assume that both nuclei are spherically symmetric.)

The motion of each of the colliding nuclei resembles that of a rigid body: the instantaneous velocity of each point of the nucleus 1 (2) is the same. Thus in the lab frame the velocity of each point of 1 vanishes, and the velocity of each point of 2 is $\hbar \boldsymbol{K}_2/M_2 = \hbar \boldsymbol{K}_{\mathrm{REL}}/\mu$, and the avarage momentum $\boldsymbol{K}_r$ of nucleons in nucleus 2 is

$$\boldsymbol{K}_r = (m/\mu)\boldsymbol{K}_{\mathrm{REL}}, \tag{2.7}$$

where $m$ is the nucleon mass. Consequently in the lab frame (see Fig. 1), the local momentum distribution at $\boldsymbol{r}$ of nucleons in nucleus 1 is the Fermi sphere (surface $F_1 = F_{10}$) centered in $O_1$, with the local Fermi momentum

$$k_{\mathrm{F}_{10}} = k_{\mathrm{F}_{10}}(r) = [3\pi^2 \varrho_1(r)/2]^{1/3}, \tag{2.8}$$

and that of nucleons in nucleus 2 is the Fermi sphere (surface $F_2 = F_{20}$) centered in $O_2$ (with $\overrightarrow{O_1 O_2} = \boldsymbol{K}_r$), with the local Fermi momentum

$$k_{\mathrm{F}_{20}} = k_{\mathrm{F}_{20}}(\boldsymbol{r}) = [3\pi^2 \varrho_2(|\boldsymbol{r} - \boldsymbol{R}|)/2)]^{1/3}. \tag{2.9}$$

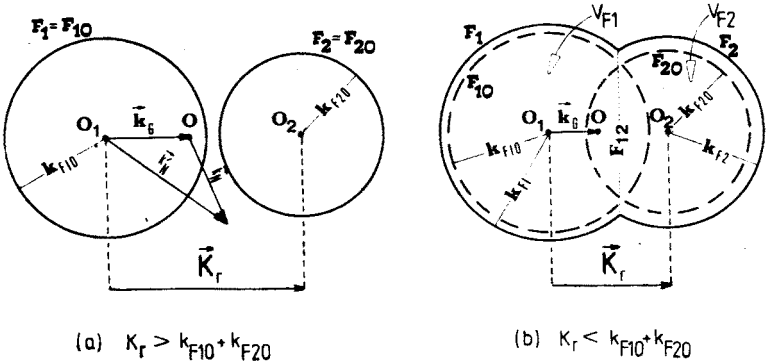


Fig. 1. The local momentum distribution in two colliding nuclei

For the combined system of nuclei 1 and 2, we obtain the local momentum distribution $n(\boldsymbol{k}'_N)$ consisting of two Fermi spheres $F_1$ and $F_2$: $n(\boldsymbol{k}'_N) = 1$ for $\boldsymbol{k}'_N$ within $F = F_1 + F_2$, and $n(\boldsymbol{k}'_N) = 0$ otherwise.

As long as $K_r > k_{F10} + k_{F20}$ (Fig. 1a), our definition of $n(\boldsymbol{k}'_N)$ presents no problems. If however $K_r < k_{F10} + k_{F20}$ (Fig. 1b), the two Fermi surfaces $F_{10}$ and $F_{20}$ overlap, and we face the problem of the double occupancy in the overlap region. We resolve this problem by increasing $k_{F10} \to k_{F1}$ and $k_{F20} \to k_{F2}$, and obtain our final momentum distribution $n(\boldsymbol{k}'_N)$ with the Fermi surface $F_1 + F_2$, with a single occupancy inside F. This reshuffling of nucleons from the original distribution $\tilde{n}$ with the Fermi surface $F_{10} + F_{20}$ (with the double occupancy in the overlap region) to our final distribution $n$ should leave the density $\varrho$ unchanged:

$$\varrho = \varrho_1 + \varrho_2 = [4/(2\pi)^3]V_F = [4/(2\pi)^3]\,(V_{F_1} + V_{F_2}), \tag{2.10}$$

where $V_F$ is the volume within F, and $V_{F1}$ ($V_{F2}$) is the volume within F to the left (right) of the plane $F_{12}$.

To determine $k_{F1}$ and $k_{F2}$, we need one equation more in addition to Eq. (2.10). Let us denote by $\boldsymbol{k}_G$ the average nucleon momentum in the local NM at $\boldsymbol{r}$ in the lab frame:

$$\boldsymbol{k}_G = \int d\boldsymbol{k}'_N n(\boldsymbol{k}'_N)\boldsymbol{k}'_N \Big/ \int d\boldsymbol{k}'_N n(\boldsymbol{k}'_N) = \begin{cases} \boldsymbol{K}_r \varrho_2/\varrho & \text{for} \quad K_r > k_{F_{10}} + k_{F_{20}}, \\ \boldsymbol{K}_r V_{F_2}/V_F & \text{otherwise.} \end{cases} \tag{2.11}$$

Before reshuffling the nucleons, in the original distribution $\tilde{n}$, we have $\boldsymbol{k}_G = \boldsymbol{K}_r \varrho_2/\varrho$ also for $K_r < k_{F10} + k_{F20}$. Let us insist that the reshuffling does not change the total momentum (equal to $\boldsymbol{k}_G$ times the number of nucleons):

$$V_{F_2}/V_F = \varrho_2/\varrho. \tag{2.12}$$

Eqs (2.12) and (2.10) are equivalent to the following two equations:

$$V_{F_1} = (4\pi/3)k^3_{F_{10}}, \qquad V_{F_2} = (4\pi/3)k^3_{F_{20}}, \tag{2.13}$$

from which both $k_{F1}$ and $k_{F2}$ may be determined (numerically).

The prescription (2.13) for determining $k_{F1}$ and $k_{F2}$ differs from the simple prescription of Beck, Muller, and Köhler [7], applied in [1–3], in which both $k_{F10}$ and $k_{F20}$ are increased by the same amount. The present prescription, applied first by Trefz, Faessler, and Dickhoff [8], has not only the advantage of preserving the total momentum in the process of the reshuffling, but it also makes the accompanying increase in the kinetic energy $\Delta\tau$ (see Eq. (2.28)) independent of the reference frame in which the kinetic energy is calculated. Actually the obvious requirement of this independence of $\Delta\tau$ leads to the present prescription. The point is that the rest frame of NM with the original momentum distribution $\tilde{n}$ coincides with the rest frame of NM with our final distribution $n$ only if $\boldsymbol{k}_G = \boldsymbol{K}_r\varrho_2/\varrho$. Notice that for $k_{F1,0} = k_{F20}$, the prescription of [7] coincides with our present prescription. Notice also, that one could preserve the total momentum while applying the prescription of [7] by properly shifting the whole distribution in momentum space.

## 2.3. The real part of $\mathscr{V}$

To simplify the presentation, we go over to the rest frame of NM, in which the total momentum vanishes. The nucleon momenta in this frame are denoted by $\boldsymbol{k}_N$. We have $\boldsymbol{k}_N = \boldsymbol{k}'_N - \boldsymbol{k}_G$ (see Fig. 1). This frame depends on $\boldsymbol{r}$ (is local). The energy density in this frame is denoted by H, and we have

$$H_{lab} = H + (\hbar^2/2m)k_G^2\varrho = H + (\hbar^2/2m)K_r^2\varrho_2^2/\varrho. \tag{2.14}$$

Let us consider normal NM (i.e., NM in its ground state) of the same density as the local density of our system. In this normal NM, the momentum distribution is $n_0(k_N) = \theta(k_F - k_N)$, where the Fermi momentum $k_F = (3\pi^2\varrho/2)^{1/3}$, and the energy density is

$$H_0^{NM} = (E_{NM}/A)\varrho = f(\varrho)\varrho, \tag{2.15}$$

where $f(\varrho) = E_{NM}/A$ is the energy per nucleon in normal NM.

The NM by which our system is locally aproximated, differs from the normal NM by the momentum distribution $n$ (the two sphere distribution in Fig. 1). We denote is energy density by $H^{NM}$, and use the approximate relation

$$\mathrm{Re}\, H^{NM} \cong H_0^{NM} + [4/(2\pi)^3] \int d\boldsymbol{k}_N [n(\boldsymbol{k}_N) - n_0(k_N)] e_0(k_N) \tag{2.16}$$

($e_0$ is the s.p. energy in normal NM), which is valid when the difference $n$-$n_0$ is small. Eq. (2.16) represents the change in the energy density caused by the redistribution of nucleons in the momentum space with unchanged s.p. energies. If we expressed the energy density through an effective two-body interaction (the $\mathscr{K}$ matrix, Eq. (2.33)), then for small $n$-$n_0$ we would obtain expression (2.16) by neglecting the change in $\mathscr{K}$ induced by the change in the momentum distribution.

For the s.p. energy $e_0$, we use the effective mass approximation:

$$e_0(k_N) = \varepsilon(k_N)/v + C, \tag{2.17}$$

where $\varepsilon(k_N) = \hbar^2 k_N^2/2m$, and $v = m^*/m$ is the ratio of the effective to the real nucleon mass. Eqs (2.15–17) lead to the following result for $\mathrm{Re}H^{NM}$:

$$\mathrm{Re}\, H^{NM} = f\varrho + (\tau - \tau_0)/v, \tag{2.18}$$

where $\tau$ and $\tau_0$ are the kinetic energy densities (in the rest frame of NM) in our system and in normal NM:

$$\tau = [4/(2\pi)^3] \int d\boldsymbol{k}_N n(\boldsymbol{k}_N)\varepsilon(k_N), \quad \tau_0 = \tau_0(\varrho) = (3/5)\varepsilon(k_F)\varrho. \tag{2.19}$$

For the semi-empirical function $f(\varrho)$, we use the form

$$f(\varrho) = (3/5)\varepsilon(k_F) + \sum_{l=3}^{5} a_l (k_F/k_{F0})^l, \tag{2.20}$$

where $k_{F0}$ is the Fermi momentum at the equilibrim density $\varrho_0$, and the coefficients $a_l$ are determined by $k_{F0}$, by the volume energy of NM, $\varepsilon_{vol} = f(\varrho_0)$, and by the compressibility $K_c = k_{F0}^2 (d^2 f/k_F^2)_0$.

For $v$, we use the form [9]:

$$v = v(\varrho) = 1/[1 + (1/v_0 - 1)\varrho/\varrho_0], \tag{2.21}$$

where $v_0 = v(\varrho_0)$.

Let us notice that in the case when the effectixe two-body interaction is assumed to be the Skyrme force SKa/b [10], Eqs (2.16)–(2.21) turn out to be exact.

So far we have approximated the energy density of our system by the energy density of the local NM. To take into account density gradient corrections, we follow Brueckner et al. [11] and add to the energy density of the local NM the gradient correction $H_\nabla$:

$$\mathrm{Re}\, H \cong \mathrm{Re}\, H^{MN} + H_\nabla, \tag{2.22}$$

where

$$H_\nabla = H_\nabla(\varrho) = \eta_W (\nabla\varrho)^2/\varrho + \eta_v (\nabla\varrho)^2, \tag{2.23}$$

with $\eta_W = \hbar^2/72m$. The first term in (2.33) is the gradient correction to the kinetic energy density, known as the Weizsäcker correction. The second term is the gradient correction to the potential energy density, in which $\eta_v$ is treated as a phenomenological parameter.

In calculating the (real) intrinsic energies $\mathscr{E}_{in}(i)$, we apply the expression:

$$\mathscr{E}_{in}(i) = \int d\boldsymbol{r}\{f(\varrho_i)\varrho_i + H_\nabla(\varrho_i)\}. \tag{2.24}$$

Eqs (2.14), (2.18), (2.22), and (2.24) allow us to calculate the real part of $\mathscr{E}_{lab}$, Eq. (2.4), and $\mathscr{E}_{in}(i)$, $i = 1,2$. Results of these calculations inserted into Eq. (2.1) give the value of $\mathscr{V}_R$. The final result for $\mathscr{V}_R$ may be presented in the form:

$$\mathscr{V}_R(E, R) = \int d\boldsymbol{r} v_R(K_r, R; \boldsymbol{r}), \tag{2.25}$$

$$v_R = f(\varrho)\varrho - f(\varrho_1)\varrho_1 - f(\varrho_2)\varrho_2 + (\tau - \tau_0)/v + H_\nabla(\varrho) - H_\nabla(\varrho_1) - H_\nabla(\varrho_2). \tag{2.26}$$

In deriving this expression, we used the relation (see Eqs (2.2), (2.7)):

$$\hbar^2 K_2^2/2M_2 = (\hbar^2 K_r^2/2m)M_2/m = (\hbar^2 K_r^2/2m) \int d\boldsymbol{r}\varrho_2(|\boldsymbol{r} - \boldsymbol{R}|). \tag{2.27}$$

Notice that $M_2/m = A_2 =$ *mass number of nucleus* 2. Of course the integral in (2.27) is not affected by using in $\varrho_2$ the argument $|\boldsymbol{r}\text{-}\boldsymbol{R}|$ instead of $r$. The same remark applies to

expression (2.24) for $\mathscr{E}_{\text{in}}$ (2). Thus we are consistent in our notation $\varrho_2 \equiv \varrho_2(|\boldsymbol{r}-\boldsymbol{R}|)$ (and $\varrho_1 = \varrho_1(r)$).

We may rewrite expression (2.26) in the form which visualizes the different factors contributing to $\mathscr{V}_{\text{R}}$:

$$v_{\text{R}} = \Delta\tau + \{(\tau-\tau_0)(1/\nu-1) + f^{\text{POT}}(\varrho)\varrho - f^{\text{POT}}(\varrho_1)\varrho_1 - f^{\text{POT}}(\varrho_2)\varrho_2\} + [H_{\nabla}(\varrho) - H_{\nabla}(\varrho_1) - H_{\nabla}(\varrho_2)]. \tag{2.28}$$

By $\Delta\tau$ we denote the increase in the kinetic energy density of the local NM caused by the Pauli blocking, i.e., the increase accompanying the reshuffling of nucleons from the momentum distribution $\tilde{n}$ to the distribution $n$:

$$\Delta\tau = \tau - \tilde{\tau} = \tau - [\tau_0(\varrho_1) + \tau_0(\varrho_2) + (\hbar^2 K_r^2/2m)\varrho_1\varrho_2/\varrho], \tag{2.29}$$

where $\tilde{\tau}$ is the kinetic energy density of NM with the distribution $\tilde{n}$. Obviously $\Delta\tau = 0$ for $K_r > k_{\text{F}10} + k_{\text{F}20}$ (no Pauli blocking).

In deriving expression (2.28), we have split the energy density of normal NM into the kinetic energy and potential energy part:

$$f(\varrho)\varrho = \tau_0(\varrho) + f^{\text{POT}}(\varrho)\varrho, \tag{2.30}$$

where obviously (see Eq. (2.20))

$$f^{\text{POT}}(\varrho) = \sum_{l=3}^{5} a_l (k_{\text{F}}/k_{\text{F}_0})^l. \tag{2.31}$$

The term $(\tau-\tau_0)(1/\nu-1)$ in (2.28) originates in the momentum dependence of the s.p. potential in NM. Thus all the terms in the curly brackets in (2.28) represent potential energy densities in homogeneous NM.

The terms in the square brackets in (2.28) represent the gradient corrections to the kinetic and potential energy densities. In the Weizsäcker approximation, the corrections to the kinetic energy density do not depend on the collision energy $E$, similarly as the corrections to the potential energy densities.

## 2.4. The imaginary part of $\mathscr{V}$

We assume that $H^{\text{NM}}$ may be expressed through an effective two-body interaction, the Brueckner reaction matrix $\mathscr{K}$:

$$H^{\text{NM}} = \tfrac{1}{2}[4/(2\pi)^3]^2 \int d\boldsymbol{k}_1 n(\boldsymbol{k}_1) \int d\boldsymbol{k}_2 n(\boldsymbol{k}_2) \langle \boldsymbol{k}|\mathscr{K}|\boldsymbol{k}\rangle, \tag{2.32}$$

where $\boldsymbol{k} = (\boldsymbol{k}_1 - \boldsymbol{k}_2)/2$. The complex $\mathscr{K}$ matrix, which depends on the conserved total momentum $2\boldsymbol{K}$ of the two nucleons 1 and 2, $\boldsymbol{K} = (\boldsymbol{k}_1 + \boldsymbol{k}_2)/2$, is defined by the equation:

$$\mathscr{K} = v_{\text{NN}} + v_{\text{NN}}[Q/(\alpha + i\eta)]\mathscr{K}, \tag{2.33}$$

where $v_{\text{NN}}$ is the NN interaction, $Q$ is the exclusion principle operator,

$$Q = [1-n(\boldsymbol{k}_1'')][1-n(\boldsymbol{k}_2'')] = [1-n(\boldsymbol{K}+\boldsymbol{k}'')][1-n(\boldsymbol{K}-\boldsymbol{k}'')], \tag{2.34}$$

and

$$\alpha = e(\boldsymbol{k}_1)+e(\boldsymbol{k}_2)-e(\boldsymbol{k}_1'')-e(\boldsymbol{k}_2''), \tag{2.35}$$

where $\boldsymbol{k}_1''$, $\boldsymbol{k}_2''$ are nucleon momenta in the intermediate states (in the rest frame of NM), and $\boldsymbol{k}'' = (\boldsymbol{k}_1''-\boldsymbol{k}_2'')/2$.

Eq. (2.33) implies the optical theorem:

$$-2\,\mathrm{Im}\,\langle \boldsymbol{k}|\mathscr{K}|\boldsymbol{k}\rangle = (2\pi)^{-2}\int d\boldsymbol{k}''Q(\boldsymbol{K}, \boldsymbol{k}'')\delta(\alpha)\,|\langle \boldsymbol{k}''|\mathscr{K}|\boldsymbol{k}\rangle|^2. \tag{2.36}$$

Now we make the following approximations:

— We assume for the s.p. energies $e$ in (2.35) the effective mass approximation with the same value of $v$ as in $e_0$, Eq. (2.17).

— We assume (for $k'' = k$) the relation

$$[m/(4\pi\hbar^2)]^2|\langle \boldsymbol{k}''|\mathscr{K}|\boldsymbol{k}\rangle|^2 = \sigma/4\pi, \tag{2.37}$$

where $\sigma = (\sigma_{nn}+\sigma_{np})/2$ ($\sigma_{nn}$ and $\sigma_{np}$ are the total nn and np cross sections). This relation is exact for the reaction matrix for two isolated nucleons, and for the isotropic NN cross section.

With these approximations, we obtain:

$$v_I \equiv \mathrm{Im}\,H^{TM} = -v(\hbar^2/2m)\,[4/(2\pi)^3]^2\int d\boldsymbol{k}_1 n(\boldsymbol{k}_1)\int d\boldsymbol{k}_2 n(\boldsymbol{k}_2)\bar{Q}(\boldsymbol{K}, k)k\sigma(k), \tag{2.38}$$

where

$$\bar{Q}(\boldsymbol{K}, k) = (4\pi)^{-1}\int d\hat{\boldsymbol{k}}Q(\boldsymbol{K}, \boldsymbol{k}). \tag{2.39}$$

Since $iv_I$ is the only imaginary quantity which enters into definition (2.1) of $\mathscr{V}$, we get for $\mathscr{V}_I$ the expression

$$\mathscr{V}_I(E, R) = \int d\boldsymbol{r}v_I(K_r, R; \boldsymbol{r}), \tag{2.40}$$

usually called the "frivolous model" expression for $\mathscr{V}_I$.

With the two-sphere momentum distribution of Fig. 1, one may obtain an analytical expression for the angle-averaged exclusion principle operator $\bar{Q}$, given in Appendix in [1]. (Let us correct two missprints there: $-\zeta$ in expression (A.22) for $\Omega$ should be replaced by $+\zeta$, and the whole right-hand side of this expression should be multiplied by $2\pi$.)

### *3. The proximity approximation*

Our final result for $\mathscr{V}$ is:

$$\mathscr{V}(E, R) = \int d\boldsymbol{r}v(K_r, R; \boldsymbol{r}), \tag{3.1}$$

where $v = v_R+iv_I$, with $v_I$ given by expression (2.38) and $v_R$ by expression (2.26) which may be written (with the help of (2.10)) in the form more convenient for our present consi-

derations:

$$v_R = [f(\varrho)-f(\varrho_0)]\varrho+(\tau-\tau_0)/\nu-(\hbar^2K_\tau^2/2m)\varrho_1\varrho_2/\varrho+H_\nabla(\varrho)$$
$$-\sum_{i=1}^{2}\{[f(\varrho_i)-f(\varrho_0)]\varrho_i+H_\nabla(\varrho_i)\}. \tag{3.2}$$

We want to show that for sufficiently large separations $R$, one may approximate our expression (3.1) for $\mathscr{V}$ by a superposition of interaction potentials between two semi-infinite slabs of NM. This is the proximity approximation, formulated in a more intuitive way by Błocki, Randrup, Świątecki, and Tsang [4]. For deriving this approximation, we need the expression for the interaction potential between two slabs of NM, defined, as the difference between the energy of two overlapping and spatially separated slabs. We start with calculating the energy of one slab of NM.

### 3.1. One slab of NM — the surface energy

We consider a semi-infinite slab of NM with the density distribution

$$\varrho(z) = \varrho_0/\{1+\exp[(z-Z)/a]\}. \tag{3.3}$$

We assume here (similarly as in [6]) that the surface has a Woods–Saxon (WS) profile.

Let us mention three ways of defining the surface of the slab (see, e.g., [12]):

(a) The half-fall distance $Z^h$:

$$\varrho(Z^h) = \varrho(-\infty)/2. \tag{3.4a}$$

(b) The sharp distance $Z^u$ of the equivalent uniform distribution $\varrho^u(z) = \varrho_0\theta(Z^u-z)$:

$$\int dz\varrho(z) = \int dz\varrho^u(z) = A_s/S, \tag{3.4b}$$

where $A_s$ is the number of nucleons in the slab.

(c) The central distance $Z^c$:

$$Z^c = \int dzz[-\varrho_0^{-1}d\varrho(z)/dz]. \tag{3.4c}$$

For the WS density (3.3), we have $Z^h = Z^u = Z^c = Z$, and thus we avoid the subtle discussion (see [4]) of the proper choice of the position of the surface of our slab. We make the obvious choice and define as the surface of our slab the plane $z = Z$, which is simultaneously the half-fall plane, the equivalent sharp plane, and the central plane.

The diffuseness of the surface of our slab is determined by $a$, connected with the 10–90% distance $t$, and with the surface width $b$ by:

$$t = (\ln 81)a, \quad b = (\pi/\sqrt{3})a, \tag{3.5}$$

where

$$b^2 = \int dz(z-Z^c)^2[-\varrho_0^{-1}d\varrho(z)/dz]. \tag{3.6}$$

To calculate the (intrinsic) energy $\mathscr{E}_{\text{in}}$ (slab) of our slab, we apply the energy-density method of Section 2:

$$\mathscr{E}_{in}(slab) = \int d\boldsymbol{r}[f(\varrho(z))\varrho(z)+H_{\nabla}(\varrho(z))]$$

$$= \int d\boldsymbol{r}\{f(\varrho_0)\varrho(z)+[f(\varrho(z))-f(\varrho_0)]\varrho(z)+H_{\nabla}(\varrho(z))\}$$

$$= \varepsilon_{\text{vol}}A_s+\gamma S, \tag{3.7}$$

where $S = \int dx \int dy$, and the surface energy parameter $\gamma$ (surface energy per unit surface, i.e., the surface tension) is

$$\gamma = \gamma_{\varrho}+\gamma_{\nabla}, \tag{3.8}$$

where $\gamma_{\varrho}$ is produced by the deviations of $\varrho$ from the uniform distribution $\varrho^{u}$ ($\int dz f(\varrho_0)\varrho = \int dz f(\varrho^{u})\varrho^{u}$—see Eq. (3.4b):

$$\gamma_{\varrho} = \int dz[f(\varrho(z))-f(\varrho_0)]\varrho(z) = aI_{\varrho}, \tag{3.9}$$

$$I_{\varrho} = \int d\zeta[f(\varrho)-f(\varrho_0)]\varrho, \quad \zeta = z/a, \tag{3.10}$$

and $\gamma_{\nabla}$ originates from the density gradient terms:

$$\gamma_{\nabla} = \int dz H_{\nabla}(\varrho(z)) = (\varrho_0/a)\,[\eta_{\text{W}}I_{\text{W}}+\varrho_0\eta_{\text{V}}I_{\text{V}}], \tag{3.11}$$

$$I_{\text{W}} = \int d\zeta(dy/d\zeta)^2/y, \quad I_{\text{V}} = \int d\zeta(dy/d\zeta)^2, \quad y = \varrho/\varrho_0. \tag{3.12}$$

For our $\varrho$, Eq. (3.1), we have $I_{\text{W}} = 1/2$ and $I_{\text{V}} = 1/6$.

We may fix the value of $a$, i.e., the diffuseness of the surface, by minimizing $\mathscr{E}_{\text{in}}$: $\partial\mathscr{E}_{\text{in}}/\partial a = 0$. This minimization leads to:

$$a = \{(\varrho_0/I_{\varrho})\,[\eta_{\text{W}}I_{\text{W}}+\varrho_0\eta_{\text{V}}I_{\text{V}}]\}^{1/2}, \tag{3.13}$$

$$\gamma_{\varrho} = \gamma_{\nabla} = \{\varrho_0 I_{\varrho}[\eta_{\text{W}}I_{\text{W}}+\varrho_0\eta_{\text{V}}I_{\text{V}}]\}^{1/2}, \tag{3.14}$$

which implies the linear relation between $\gamma$ and a:

$$\gamma = 2I_{\varrho}a. \tag{3.15}$$

### 3.2. Two slabs of NM

We consider two slabs of NM, 1 and 2, facing each other and moving against each other with the relative momentum $\boldsymbol{K}_{\text{REL}}$. Their instantaneous distance $Z_{12}$ is defined as the distance between the half-fall planes of the two slabs. We choose the $z$-axis perpendicular to the two planes, direct it from slab 1 to slab 2, and place the origin of the coordinate system at the half-fall point of slab 1. The density distributions in slab 1 and slab 2 are:

$$\varrho_1(z) = \varrho_0/\{1+\exp[z/a]\}, \quad \varrho_2(z) = \varrho_0/\{1+\exp[(Z_{12}-z)/a)]\}. \tag{3.16}$$

The density $\varrho$ of the combined system of the two slabs (in the frozen density model) is:

$$\varrho(z) = \varrho_1(z)+\varrho_2(z). \tag{3.17}$$

We denote by $\mathscr{U}(E, Z_{12}) = \mathscr{U}_R + i\mathscr{U}_I = \mathscr{V}/S$ the optical potential per unit surface for the two slabs. By applying expressions (3.1–2) and (3.7), we get:

$$\mathscr{U}_R(E, Z_{12}) = \int dz u_R(K_r, Z_{12}; z) - 2\gamma, \tag{3.18}$$

$$u(K_r, Z_{12}; z) = [f(\varrho) - f(\varrho_0)]\varrho + (\tau - \tau_0)/\nu - (\hbar^2 K_r^2/2m)\varrho_1\varrho_2/\varrho + H_v(\varrho), \tag{3.19}$$

and

$$\mathscr{U}_I(E, Z_{12}) = \int dz v_I(K_r, Z_{12}; z), \tag{3.20}$$

where $v_I$ is given in Eq. (2.38), in which the density distributions are now those of Eqs (3.16–17).

We follow [4], and define the dimensionless proximity function

$$\phi(E, s) = \phi_R + i\phi_I = \mathscr{U}/2\gamma, \tag{3.21}$$

where $s = Z_{12}/a$. We have:

$$\phi_R(E, s) = \int dz u_R/2\gamma - 1, \quad \phi_I = \int dz v_I/2\gamma. \tag{3.22}$$

Notice that our proximity function $\phi$ is complex and energy dependent. Only for $E = 0$, $\phi_I = 0$, and our $\phi(0, s) = \phi_R(0, s)$ becomes the pure real proximity force function considered in [4].

### 3.3. The HI optical potential

We consider two spherical nuclei $i = 1$ and $i = 2$ with mass numbers $A_i$ and with the WS density distributions:

$$\varrho_i(r) = \varrho_0/\{1 + \exp[(r - R_i)/a]\}. \tag{3.23}$$

We assume that $R_i \gg a$. In this case, the half-fall radius $R_i^h = R_i$, and the central radius $R_i^c = R_i$. (For $R_i \gg a$ the definition of $R^c$ coincides with definition (3.4c) of $Z^c$.) The equivalent uniform distribution $\varrho_i^u = \varrho_0\theta(R_i^u - r)$ has the sharp radius $R_i^u = r_0 A_i^{1/3}$ (where $r_0 = (4\pi\varrho_0/3)^{-1/3}$), which is determined from the condition (compare (3.4b))

$$\int_0^\infty dr r^2 \varrho_i(r) = \int_0^\infty dr r^2 \varrho_i^u(r), \tag{3.24}$$

which leads to (see, e.g., Elton [13]):

$$R_i \cong R_i^u[1 - \tfrac{1}{3}(\pi a/R_i^u)^2] = r_0 A_i^{1/3}[1 - \tfrac{1}{3}(\pi a/r_0)^2 A_i^{-2/3}]. \tag{3.25}$$

Thus we have $R_i^h = R_i^c = R_i < R_i^u$.

We start with expression (3.1) for $\mathscr{V}$, which we write in the form:

$$\mathscr{V}(E, R) = \int dx \int dy \int dz v(K_r, R; r_\perp, z) = \int dx \int dy \tilde{v}(K_r, R; r_\perp), \tag{3.26}$$

where

$$\tilde{v}(K_r, R; r_\perp) = \int dz v(K_r, R; r_\perp, z). \tag{3.27}$$

Similarly as in Section 2.2, we place the origin of the coordinate system at the center of nucleus 1, and direct the $z$-axis toward the center of nucleus 2. Because of the cylindrical symmetry, $v$ depends (through the densities $\varrho_1$ and $\varrho_2$ — see Eq. (2.6)) only on $z$ and $r_\perp = (x^2+y^2)^{1/2}$.

We want to show that for sufficiently large separations $R$ of the two nuclei, the exact (within our energy-density approach) expression for $\mathscr{V}$, Eqs (3.26–27), goes over into the proximity approximation of [4]. We consider such large separations $R$, that the two nuclei do not overlap over an appreciable fraction of their volume, which means that approximately $R \gtrsim R_1 + R_2$ or at least $R$ should not be much smaller than $R_1 + R_2$. For such values of $R$, we have in the overlap region

$$r_\perp \ll R_1, \quad \text{and} \quad r_\perp \ll R_2. \tag{3.28}$$

Since only the overlap region contributes to $\mathscr{V}$, in approximating $\tilde{v}$, we shall assume inequalities (3.28) also outside the overlap region. Of course, the nuclear surface is diffused and the definition of the overlap region is not very precise. We may define it as that part of the configuration space whose contribution to $\mathscr{V}$ is dominant, and we consider such large values of $R$ that (3.28) is satisfied in it.

The densities $\varrho_1$ and $\varrho_2$, which enter into $\tilde{v}(K_r, R; r_\perp)$ (see Eqs (3.2), (2.38)), are:

$$\varrho_1(r) = \varrho_0/(1+\exp[(r_\perp^2+z^2)^{1/2} - R_1]/a\}) \equiv \tilde{\varrho}_1(z),$$

$$\varrho_2(|\boldsymbol{r}-\boldsymbol{R}|) = \varrho_0/(1+\exp\{[(r_\perp^2+(z-R)^2)^{1/2} - R_2]/a\}) \equiv \tilde{\varrho}_2(z). \tag{3.29}$$

First let us discuss $\tilde{\varrho}_1(z)$ which as a function of $z$ does not have the WS shape of the original density $\varrho_1(r)$, Eq. (3.23). For the half-fall distance $\tilde{Z}_1^h$ and the 10–90% distance $\tilde{t}_1$ of the distribution $\tilde{\varrho}_1(z)$, we get (under assumption (3.28)):

$$\tilde{Z}_1^h = R_1 - r_\perp^2/2R_1, \quad \tilde{t}_1 = t[1+(r_\perp/R_1)^2/2], \tag{3.30}$$

where $t = (\ln 81)\, a$ is the 10–90% distance of the original WS distribution. The inequality $\tilde{t}_1 > t$ simply reflects the fact that for $r_\perp > 0$ the nuclear surface is not perpendicular to the $z$-axis, and the density at $r_\perp > 0$ as a function of $z$, $\tilde{\varrho}_1(z)$, has a more diffused profile than the original density $\varrho_1(r)$. However for $r_\perp \ll R_1$ the surface remains almost perpendicular to the $z$-axis, thus the difference between $\tilde{t}_1$ and $t$ is very small (of order $(r_\perp/R_1)^2$), and we neglect this difference. Furthermore, we approximate $\tilde{\varrho}_1(z)$ by an equivalent WS distribution with the same half-fall distance $\tilde{Z}_1^h$ and the same 10–90% distance $\tilde{t}_1 \cong t$ as the distribution $\tilde{\varrho}_1(z)$:

$$\tilde{\varrho}_1(z) \cong \varrho_0/(1+\exp\{[|z| - (R_1 - r_\perp^2/2R_1)]/a\}). \tag{3.31}$$

Of course for $r_\perp = 0$ the nuclear surface is perpendicular to the $z$-axis and Eq. (3.31) is exact.

We proceed with $\tilde{\varrho}_2(z)$ in an analogous way (the procedure is identical with $z' = z-R$), and get:

$$\tilde{\varrho}_2(z) \cong \varrho_0/(1+\exp\{[|R-z|-(R_2-r_\perp^2/2R_2)]/a\}). \tag{3.32}$$

Within our small overlap region, we have $|z| = z$ and $|R-z| = R-z$. Since values of $\tilde{\varrho}_1$ and $\tilde{\varrho}_2$ outside the oxerlap region are irrelevant for the resulting value of $\tilde{v}$, we may safely remove the absolute value signs in (3.41–42), and thus we get our final approximation:

$$\tilde{\varrho}_1(z) \cong \varrho_0/(1+\exp\{[z-(R_1-r_\perp^2/2R_1)]/a\}), \tag{3.33}$$

$$\tilde{\varrho}_2(z) \cong \varrho_0/(1+\exp\{[(R-R_2+r_\perp^2/2R_2)-z]/a\}). \tag{3.34}$$

After lifting the absolute value signs in (3.31–32), we have $\tilde{\varrho}_1 \cong \varrho_0$ for $z < 0$, and $\tilde{\varrho}_2 \cong \varrho_0$ for $z > R$. Thus the new densities $\tilde{\varrho}_1$ and $\tilde{\varrho}_2$, Eqs (3.33–34) represent the densities of two semi-infinite slabs of NM facing each other, and separated by the distance

$$Z_{12} = R-R_1-R_2+r_\perp^2/2R_{12}, \tag{3.35}$$

where $R_{12} = R_1R_2/(R_1+R_2)$. Hence, according to Section 3.2, we have:

$$\tilde{v} = \mathcal{U}(E, Z_{12}), \tag{3.36}$$

where $\mathcal{U} = \mathcal{U}_R + i\mathcal{U}_J$ is the interaction potential per unit surface between two slabs with the density distributions (3.33–34) (see expressions (3.18) and (3.19) for $\mathcal{U}_R$ and $\mathcal{U}_I$).

Although expressions (3.33–34) (and thus expression (3.36)) have been derived under assumption (3.28), we shall use them also in regions of large values of $r_\perp$, because these regions give negligible contributions to $\tilde{v}$, provided $R$ is not too small.

For our approximate optical potential, which we denote by $\mathcal{V}^P$, we get

$$\mathcal{V}(E, R) \cong \mathcal{V}^P(E, R) = 2\pi \int_0^\infty dr_\perp r_\perp \mathcal{U}(E, Z_{12}) = 4\pi a\gamma R_{12}\Phi(E, s_0), \tag{3.37}$$

where

$$\Phi(E, s_0) = \int_{s_0}^\infty ds\phi(E, s), \tag{3.38}$$

where $\phi(E, s)$ is the complex and energy dependent proximity function (see Eqs (3.21–22), and

$$s_0 = (Z_{12})_{\min}/a = (R-R_1-R_2)/a. \tag{3.39}$$

For $E = 0$, $\mathcal{V}^P = \mathcal{V}_R^P$ coincides with the proximity potential of [4].

### *4. Results and discussion*

First let us list the input parameters of our calculations.

As NM parameters, we use: $k_{F0} = 1.35$ fm$^{-1}$($\varrho_0 = 1.662$ fm$^{-3}$, $r_0 = 1.128$ fm), $\varepsilon_{vol} = -15.8$ MeV, $K_c = 235$ MeV, and $v_0 = 0.83$. This value of $v_0$ has been determined

by Johnson, Horen, and Mahaux [14] in their analysis of the nucleon-nucleus optical potential with dispersion relation constraint.

For the total NN cross section $\sigma = (\sigma_{nn}+\sigma_{np})/2$, we use the parametrization of Metropolis et al. [15] when the laboratory energy $E_L > 20$ MeV. For $E_L < 20$ MeV, we use the effective range approximation with the following values (in fm) of the respective singlet (s) and triplet (t) scattering lengths ($a$) and effective ranges ($r$): $a_{snn} = -16.1$, $r_{snn} = 3.2$, $a_{snp} = -23.7$, $r_{snp} = 2.704$, $a_{tnp} = 5.4$, $r_{tnp} = 1.73$.

We use the WS profile for the surface, Eqs (3.1), (3.20), with the 10–90% distance $t = 2.5$ fm ($a = 0.5689$ fm, $b = 1.0319$ fm). In $H_\nabla$, Eq. (2.23), we use the value of $\eta_\nabla = 22$ MeV fm$^5$, fitted in [2] to the binding energies of $^{16}$O and $^{40}$Ca. These values of $a$ and $\eta_\nabla$, inserted into expressions (3.7) and (3.9), give for the surface tension a reasonable result: $\gamma = 0.9796$ MeV fm$^{-2}$.

Let us make a comment on the minimization procedure of determining $t = (\ln 81)a$ and $\gamma$, Eqs (3.13–14). To get from Eq. (3.13) for $t$ the empirical value of 2.5 fm, we would need $\eta_\nabla = 78$ meV fm$^5$, and would get for $\gamma$ a too large value of 1.4 MeV fm$^{-2}$. On the other hand to get $\gamma = 1$ MeV fm$^{-2}$, we would need $\eta_\nabla = 33$ MeV fm$^5$, and would get for $t$ a too small value of 1.75 fm. (For $\eta_\nabla = 22$ MeV fm$^5$, we would get $\gamma = 0.87$ MeV fm$^{-2}$ and $t = 1.5$ fm.) The failure of obtaining in the minimization procedure simultaneously reasonable (empirical) values of $t$ and $\gamma$ is due probably to the simiplified WS form of our density distribution, and of our $H_\nabla$ (which leads to the linear relation, Eq. (3.15)). In this situation, we did not apply the minimization procedure, and instead considered $t$ and $\eta_\nabla$ (and thus $\gamma$) as two independent adjustable parameters.

Our gradient correction $H_\nabla$ to the energy density, Eq. (2.23), contains the Weizsäcker term. This turns out not to be important. All our results would be changed only slightly, if instead of $H_\nabla$ we used $H_\nabla^0 = \eta_\nabla^0(\nabla\varrho)^2$, provided the surface tension remained unchanged ($\eta_\nabla^0 = \eta_\nabla + 3\eta_W/\varrho_0 = 32.397$ MeV fm$^5$).

As pointed out in Section 2, the relative momentum $K_{REL} = K_{REL}(R)$ depends on $R$, Eq. (2.3). Hence also $K_r = (m/\mu)K_{REL}$ depends on $R$, $K_r = K_r(R)$. In the present calculations, we neglect this $R$ dependence of $K_r$, and put $K_r = K_r(\infty)$. This appears justified in discussing the proximity approximation which is an approximation for large separations $R$, where the difference between $K_r(R)$ and $K_r(\infty)$, discussed in [2] and [3], is less important. Let us add that if we took into account the $R$ dependence of $K_r$, we would loose the simplicity of the proximity approximation.

The connection between $E_{LAB}/A_2$ (the kinetic energy of the projectile nucleus 2 per projectile nucleon in the LAB system) and $K_r = K_r(\infty)$ (in fm$^{-1}$) is:

$$E_{LAB}/A_2 = \hbar^2 K_r^2/2m = 20.7\, K_r^2 \text{ MeV}. \tag{4.1}$$

For the CMS kinetic energy $E$, we have:

$$E = (A_1A_2/(A_1+A_2))\hbar^2 K_r^2/2m. \tag{4.2}$$

Our result obtained for the proximity function at $E = 0$, $\phi = \phi_R$, is shown as the solid curve A in Fig. 2. To compare our result with that of [4], where the proximity function

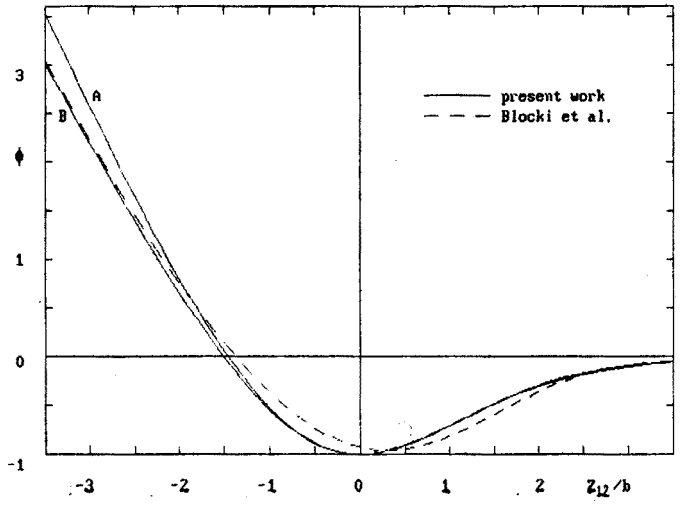


Fig. 2. The proximity force function $\phi = \phi_R$ versus $Z_{12}/b$ at $E = 0$

has been calculated as a function of $Z_{12}/b$, we display on the abcissa $Z_{12}/b = (a/b)s = (\sqrt{3}/\pi)s$. Notice that with our WS densities (3.16), at $Z_{12} = 0$ the total density of the overlapping slabs is exactly constant:

$$\varrho(z) = \varrho_1(z) + \varrho_2(z) \equiv \varrho_0 \quad \text{for} \quad Z_{12} = 0. \tag{4.3}$$

This means that at $Z_{12} = 0$ the energy of the combined system differs from the sum of the energies of the isolated slabs only by their surface energies, thus the interaction potential $\mathcal{U} = -2\gamma$, and $\phi = \mathcal{U}/2\gamma = -1$. Obviously the energy of the combined system of two slabs (hence also $\phi$) reaches its minimum when the density distribution is uniform and equal $\varrho_0$, and this happens when $Z_{12} = 0$. For large negative $s$, a region of double density $\varrho = 2\varrho_0$ is formed, which leads to a repulsive $\phi \sim (\varrho_0 a/\gamma)\,[f(2\varrho_0) - f(\varrho_0)]\,|s|$.

The proximity function $\phi$ (at $E = 0$) calculated in [4] is shown as the broken curve in Fig. 2. In [4], the Thomas-Fermi approximation with the Seyler–Blanchard effective NN interaction [16] was applied. The density distribution of one slab was determined as the equilibrium distribution, with the resulting values of $b = 0.872$ fm and $\gamma = 1.017$ MeV fm$^{-2}$, which differ from our values. Let us also notice that the Seyler–Blanchard interaction leads to NM parameters: $r_0 = 1.2049$ fm, $\varepsilon_{\text{vol}} = -15.677$ MeV, $K_c = 294.80$ MeV [17], which also differ from our NM parameters. To make a comparison with [4] more meaningful, we have calculated $\phi$ with these Seyler–Blanchard NM parameters, and with $b = 0.872$ fm ($t = 2.113$ fm). Furthermore, we applied the minimization procedure, Eqs. (3.13–15), which lead to $\eta_V = 73$ MeV fm$^5$ and $\gamma = 1.113$ MeV fm$^5$. The result is shown as the solid curve B in Fig. 2, which for increasing negative $Z_{12}$ approaches the result of [4]. The remaining small discrepancy for $Z_{12} \cong 0$ appears to be due to the difference in the density profiles. For the profile of the equilibrium distribution of one slab obtained in [4] (which differs from the simple WS profile which we assume), there is no such separation $Z_{12}$ for which Eq. (4.3) would be exactly satisfied. This explains

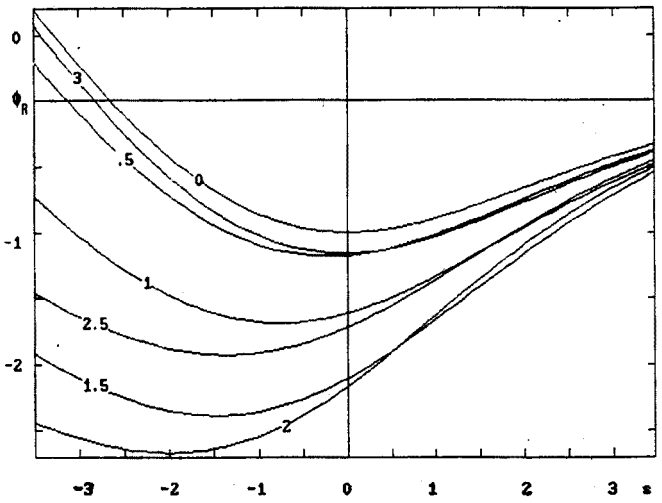


Fig. 3. The proximity function $\phi_R$ versus $s$ for $K_r = 0(0.5)3$ fm$^{-1}$

why $\phi$ calculated in [4] is never equal exactly $-1$, and reaches its minimum at separation $Z_{12}$ slightly different from zero. Notice also that the central plane and the half-fall plane (which coincide in the case of our WS distribution) differ in the case of a more general distribution. This introduces certain ambiguity into the comparison of our results with those of [4] (where $Z_{12}$ appears to be the distance between the central planes of the two slabs).

The dependence of $\phi_R$ on $K_r$, i.e., on the energy $E$ ($E/A_1 = \frac{1}{2}\hbar^2 K_2^r/2m$ — see Eq. (4.2)) is shown in Fig. 3. As $K_r$ increases, the role of the Pauli blocking and thus the repulsive contribution $\Delta\tau$, Eq. (2.28), decreases. Consequently the interaction potential between the two slabs, i.e., $\phi_R$ becomes more attractive and its minimum is shifted towards smaller (more negative) values of $s$. On the other hand, there is the repulsive potential energy contribution $(\tau - \tau_0)(1/v - 1)$ in Eq. (2.28), which increases with increasing $K_r$. For $K_r \gtrsim 2$ fm$^{-1}$ it becomes dominant, and consequently $\phi_R$ becomes again less attractive. Notice that $\Delta\tau \equiv 0$ for $K_r > 2k_{F0} = 2.7$ fm$^{-1}$.

For $K_r > 0$, the proximity function is complex. Its imaginary part $\phi_I$ for $K_r = 1$ and 2 fm$^{-1}$ is shown in Fig. 4. It represents the absorptive potential which arises from the two-body mechanism of incoherent NN collisions. Obviously $|\phi_I|$ increases with increasing $K_r$, because more and more phase space allowed by the exclusion principle is available for the final states in the NN scattering.

Our derivation of the proximity approximation for the optical potential $\mathcal{V}(E, R)$, as well as the original derivation of $\mathcal{V}^P(E = 0, R)$ in [4], suggest that $\mathcal{V}^P \cong \mathcal{V}$ for $R - R_1 - R_2 \gtrsim 0$. Furthermore, we used the assumption $R_i \gg a$, i.e., that nuclei are "leptodermous", which implies that neither nucleus should be very light. To see precisely how good is the proximity approximation, we compare the results obtained for $\mathcal{V}$ with the energy-functional method of Section 2 (which we call "exact") with the results obtained for $\mathcal{V}^P$ with the proximity approximation of Section 3 (within the same energy-functional

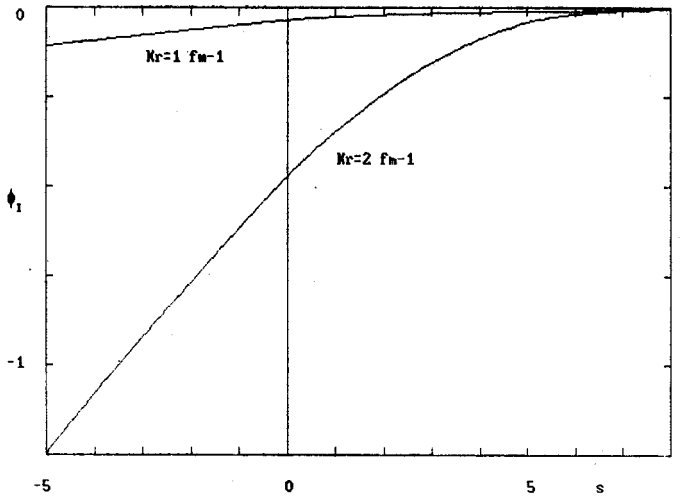


Fig. 4. The proximity function $\phi_1$ versus $s$ for $K_r = 1, 2\,\mathrm{fm}^{-1}$

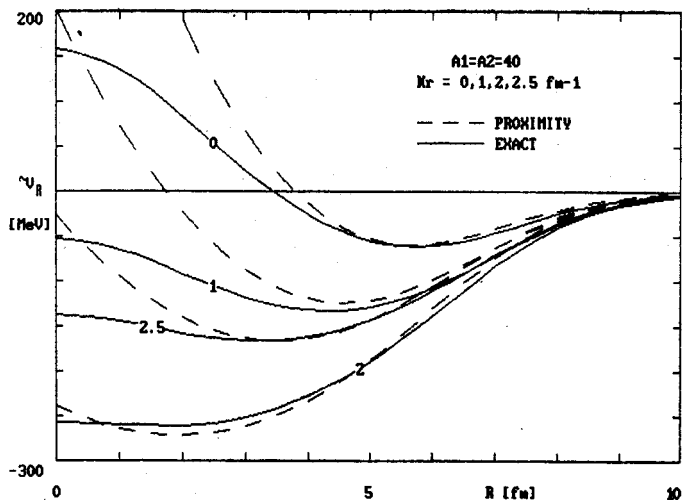


Fig. 5. $\mathscr{V}_R$ for $^{40}Ca-^{40}Ca$ for the indicated values of $K_r$

method). We consider the case of two equal spherical nuclei: $A_1 = A_2$, $R_1 = R_2$, $R_{12} = R_1/2$.

Results obtained for $\mathscr{V}(E, R)$ and $\mathscr{V}^{\mathrm{P}}(E, R)$ for two $^{40}Ca$ nuclei are shown in Figs 5 and 6. In the present investigation of the proximity approximation, we use the schematic WS density, whereas in [2] the experimental density was used. Furthermore, our present value of the effective mass $v_0 = 0.83$ is greater than the value 0.7 used in [2]. These are the main reasons for some differences between the present results for $\mathscr{V}$ and those obtained in [2]. (Also the $R$ dependence of $K_r$, considered in [2], is neglected in the present work, and our present prescription for constructing the two-sphere momentum distribution

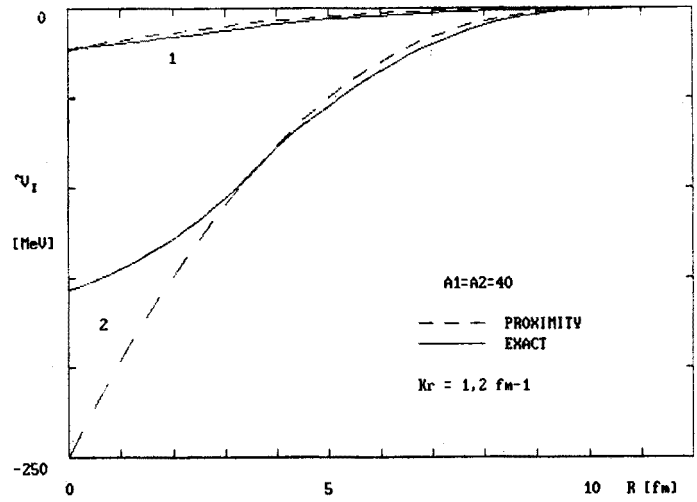


Fig. 6. $\mathcal{V}_I$ for $^{40}Ca-^{40}Ca$ for $K_r = 1,2\,\mathrm{fm}^{-1}$

differs from the prescription applied in [2].) The dependence of $\mathcal{V}$ on $R$ and $E$ (or $K_r$) reflects the dependence of $\phi$ on $s$ and $K_r$ discussed before.

Results for the proximity approximation $\mathcal{V}^P$ (the broken curves in Figs 5 and 6) are reasonably close to the exact results for sufficiently large separations $R$ of the two ions. For small values of $R$, replacement (3.34) and (3.35) of the densities $\tilde{\varrho}_i(z)$ by densities of semi-infinite slabs is obviously not justified and leads to serious discrepancies between $\mathcal{V}^P$ and $\mathcal{V}$. The error committed by this replacement depends on the behaviour of $\phi(s)$ for large negative $s$, which depends on $K_r$ (see Figs 3 and 4). Thus the magnitude of the discrepancies between $\mathcal{V}^P$ and $\mathcal{V}$ at small values of $R$ also depends on $K_r$.

The main consequence and advantage of the proximity approximation, Eqs (3.37–39), is that the optical potential $\mathcal{V}^P$ in this approximation is the product of the geometrical factor $\sim R_{12}$ and of the universal (energy dependent) function $\Phi$ of $R-R_1-R_2$. Thus the best way of investigating the proximity approximation is to plot $\mathcal{V}/R_{12} = \mathcal{V}/(R_1/2)$ as a function of $R-R_1-R_2 = R-2R_1$. This is done in Figs 7–9. If the scaling low implied by the proximity approximation is correct, the results for $\mathcal{V}/(R_1/2)$ as functions of $R-2R_1$ should not depend on $A_1$. (A direct verification of this scaling low in the energy--density formalism at $E = 0$ has been approximately demonstrated by Ngô et al. [18] and Brink and Stancu [19].)

In Fig. 7, we show the results obtained for $\mathcal{V}_R/(R_1/2)$ at $E = 0$ for $A_1 = 16$, 40, and 125 as functions of $R-2R_1$. Our exact results, the solid curves for $A_1 = 40$ and 125 are indeed very close to each other for $R - 2R_1 \gtrsim -3$ fm, i.e., even before reaching the minimum. On the other hand, the $A_1 = 16$ curve for the much lighter $^{16}O$ nuclei joins the two other solid curves much later (at $R-2R_1 \gtrsim -1$ fm, i.e., beyond the minimum). We conclude that our exact results for not too light nuclei ($A_1 > 16$) and not too large overlaps ($R-2R_1 \gtrsim -3$ fm) show indeed the scaling low implied by the proximity approximation. We see also that within this range of overlaps the exact results stay reasonable

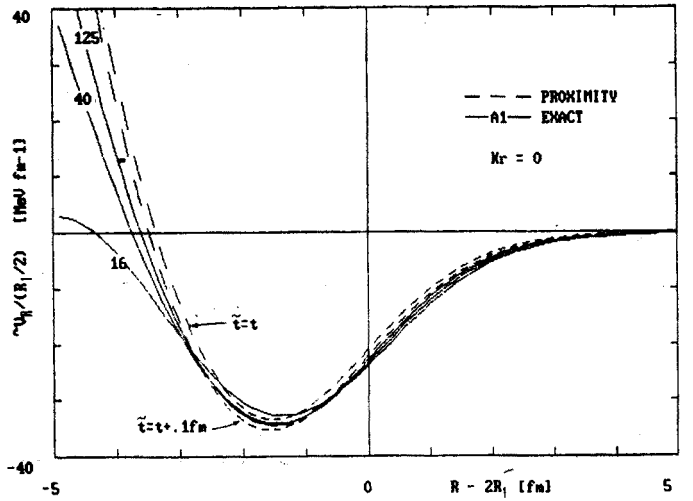


Fig. 7. $\tilde{\gamma}_R/(R_1/2)$ for two equal nuclei versus $R-2R_1$ at $E=0$

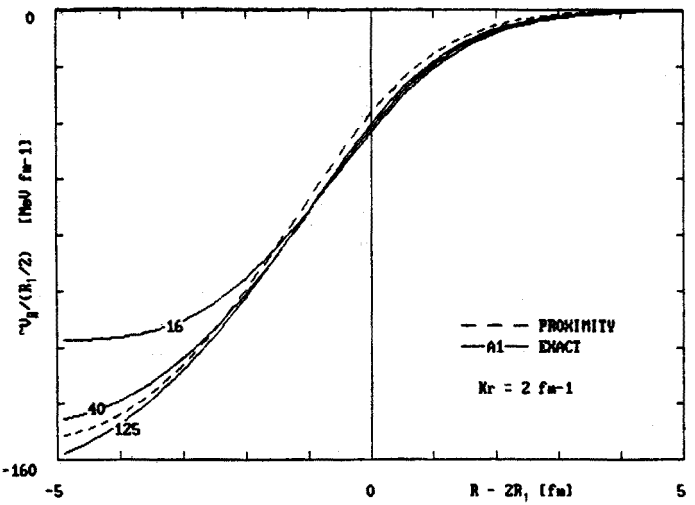


Fig. 8. $\tilde{\gamma}_R/(R_1/2)$ for two equal nuclei versus $R-2R_1$ for $K_r = 2\,\mathrm{fm}^{-1}$

close to our proximity approximation results (the broken $\tilde{t}=t$ curve). However, even for positive values of $R-2R_1$, there is a visible difference between the exact curves and our proximity approximation curve. To explain this difference, let us notice that in deriving the proximity approximation we assumed that the 10–90% distance $\tilde{t}$ of the distributions $\tilde{\varrho}_1(z)$ and $\tilde{\varrho}_2(z)$ is the same as the 10–90% distance $t$ of the original WS distribution. However, since the surface of the two nuclei are not exactly parallel, we have $\tilde{t} > t$. Eq. (3.30). To see the effect of this increased diffuseness of the surface elements of the two nuclei facing each other, we also show in Fig. 7 the proximity approximation curve obtained with $\tilde{t} = t+0.1$ fm, and see that indeed it is closer to the exact results than the $\tilde{t}=t$ curve.

Our results for $\tilde{\gamma}_R/(R_1/2)$ at $K_r = 2\,\mathrm{fm}^{-1}$ are shown in Fig. 8. The situation here is

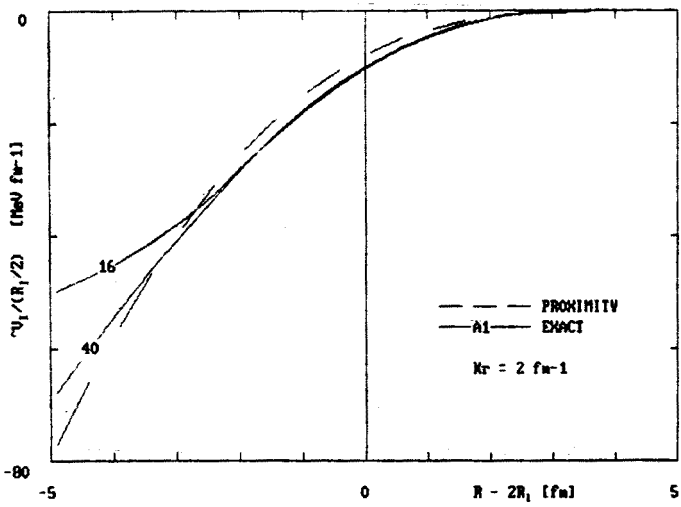


Fig. 9. $\mathcal{V}_I/(R_1/2)$ for two equal nuclei versus $R-2R_1$ for $K_r = 2\,\mathrm{fm}^{-1}$

similar as at $K_r = 0$. The only difference is that at $K_r = 2\,\mathrm{fm}^{-1}$ the scaling low applies to larger negative values of $R-2R_1$. Notice that $\mathcal{V}_R$ reaches its maximal depth at $K_r \cong 2\,\mathrm{fm}^{-1}$.

Our results for $\mathcal{V}_I/(R_1/2)$ at $K_r = 2\,\mathrm{fm}^{-1}$ for $A_1 = 16$ and 40 are shown in Fig. 9. Again the situation is similar as in the case of $\mathcal{V}_R$. We see that the proximity approximation and the scaling low work with about the same accuracy in the case of $\mathcal{V}_I$ as in the case of $\mathcal{V}_R$.

We conclude that for sufficiently small overlaps of the two colliding nuclei, the proximity approximation is applicable as well in the case of $E = 0$, as in the case of $E > 0$. At $E > 0$ the optical potential $\mathcal{V}$ is complex, and the proximity approximation may be applied equally well to both real and imaginary parts of $\mathcal{V}$. The main advantage of the proximity approximation is, that to obtain within this approximation $\mathcal{V}$ for different pairs of colliding nuclei, it is sufficient to calculate (at each energy) one universal complex function $\Phi(E, s_0)$, Eq. (3.38) (and apply expression (3.37)). In the case of $\mathcal{V}_R$, the nice intuitive picture of the nucleus-nucleus interaction potential offered by the proximity approximation is probably more important than the computational simplicity, because our exact expression for $\mathcal{V}_R$, Eqs (2.25–26) is in itself very simple (the application of Eq. (2.25) requires only a two-dimensional integration). On the other hand in the case of $\mathcal{V}_I$, the computational simplification introduced by the proximity approximation saves a lot of computing time. Namely expressions (2.38) and (2.40) for $\mathcal{V}_I$ require performing a seven-dimensional integration.

Let us summarize the main points of the present paper:

— We have outlined a simple energy-density formulation of the energy dependent complex optical potential $\mathcal{V}$ for HI collisions, in which $\mathcal{V}$ is expressed through saturation properties of NM and the NN cross section.

— We introduced into the energy-density formulation approximations which are reasonable when the two ions do not overlap too much, and derived a generalized proximity approximation valid for both real and imaginary parts of $\mathscr{V}$.

— We tested the accuracy of the generalized proximity approximation by comparing the results for $\mathscr{V}$ obtained with the energy-density formalism exactly with those obtained with the proximity approximation.

## REFERENCES


[1] J. Dąbrowski, H. S. Köhler, *Nucl. Phys.* **A489**, 303 (1988).
[2] J. Dąbrowski, *Acta Phys. Pol.* **B20**, 61 (1989).
[3] J. Dąbrowski, H. S. Köhler, *Nucl. Phys.* **A499**, 413 (1989).
[4] J. Błocki, J. Randrup, W. J. Świątecki, C. F. Tsang, *Ann. Phys. (N. Y.)* **105**, 427 (1977).
[5] K. A. Brueckner, J. R. Buchler, M. M. Kelly, *Phys. Rev.* **173**, 944 (1968).
[6] S. A. Moszkowski, *Nucl. Phys.* **A309**, 273 (1978).
[7] F. Beck, K.-H. Müller, H. S. Köhler, *Phys. Rev. Lett.* **105B**, 205 (1981).
[8] M. Trefz, A. Faessler, W. W. Dickhoff, *Nucl. Phys.* **A443**, 499 (1985).
[9] B. Friedman, V. R. Pandharipande, *Phys. Lett.* **B100**, 205 (1981).
[10] H. S. Köhler, *Nucl. Phys.* **A258**, 301 (1976).
[11] K. A. Brueckner, J. L. Buchler, S. Jorna, R. L. Lombard, *Phys. Rev.* **171**, 1188 (1968).
[12] W. D. Myers, *Nukleonika* **21**, 3 (1976).
[13] L. R. B. Elton, *Nuclear Sizes*, Oxford University Press, 1961.
[14] C. H. Johnson, D. J. Horen, C. Mahaux, *Phys. Rev.* **C36**, 2252 (1987).
[15] N. R. Metropolis et al., *Phys. Rev.* **110**, 204 (1958).
[16] R. G. Seyler, C. H. Blanchard, *Phys. Rev.* **124**, 227 (1961); **131**, 355 (1963).
[17] W. D. Myers, W. J. Świątecki, *Ann. Phys. (N. Y.)* **55**, 395 (1969).
[18] C. Ngô, B. Tamain, M. Beiner, R. L. Lombard, D. Mass, H. H. Deubler, *Nucl. Phys.* **A256**, 237 (1975).
[19] D. M. Brink, Fl. Stancu, *Nucl. Phys.* **A299**, 321 (1978).